Evaluation of local stress and strain state at notch root by means of a new method valid for multiaxial random loadings

Thibault Herbland, Georges Cailletaud, Stéphane Quilici

Evaluation of Local Stress and Strain State at Notch Root by Means of a New Method Valid for Multiaxial Random Loadings

T. Herbland[1,2], *G. Cailletaud*[2], *S. Quilici*[2]
[1]*Cetim, Senlis, France;*
[2]*Centre des Matériaux, Mines–ParisTech, CNRS UMR 7633, 91003 Evry Cedex, France*
E-mail : thibault.herbland@ensmp.fr

Abstract

Neuber type methods are widely used to predict the local stress-strain behaviour at notch root in specimens or industrial components. Some limitations of these methods are pointed out in the present paper, especially when the global loading is multiaxial and/or random. A fully new approach is then presented: it introduces a phenomenological model describing the development of residual stresses that can be calibrated by reference to Eshelby's type approaches. A tensorial variable is used for this purpose. Its evolution rule allows us to represent the stress redistribution at the surface of the component. Isotropic and anisotropic constitutive equations are accepted for the description of the material behaviour. It has been successfully used for several complex situations (cyclic, multiaxial, random loadings).

1 Introduction

Fatigue analysis of mechanical components is divided into several steps. The first one consists in evaluating local stresses and/or strains. Either finite element method or accelerated computation methods can be used for that purpose. The former gives an accurate solution but is time consuming, especially for the case of non linear behavior and complex structures. The latter computes an approximate solution but within a short time. There are several kinds of accelerated computation methods. Some of them determine the mechanical steady state: the cycle skip method [1], or the direct cyclic method [2]. They are useful for the case of constant amplitude loading, or when the steady state is reached quickly. But in case of variable-amplitude loading, a significant part of the fatigue life is consumed before the steady state appears, if it does. Moreover, fatigue initiation sites are often known, so that there is no need to compute the whole structure. That is why Neuber-type methods can be more interesting as they are dedicated to the evaluation of stress concentrations,

for instance in notches. The paper wishes to address this class of methods. They use the local stresses and strains computed at the notch tip from an elastic finite element analysis (FEA) to evaluate the elastic-plastic ones, and can be applied to variable-amplitude fatigue loading. Neuber [3] formulated his theory for uniaxial stress states in 1961. Then, Molski and Glinka [4] proposed an alternative approach also for uniaxial stress states. Other researchers [5] proposed models extensions valid for multiaxial stress states, but only for some specific geometries. Lately, Buczynski and Glinka [6] proposed an incremental model that gives rather good agreement with FEA results but fails for some components of the stress or strain tensors. The model proposed in this study is derived from an adjustable scale transition rule. It considers the material element in the notch root as a plastic inclusion in a less loaded homogeneous medium. The validity of the approach has been tested on various loading paths, like constant loading with several stress ratios, in torsion, tension and combined proportional tension-torsion.

2 Model description

Using the solution of the problem of a spherical inclusion I in an infinite matrix M, Kröner's model allows to determine the relation between the average stress tensor ($\underset{\sim}{\sigma}$), the stress tensor in an inclusion of an aggregate ($\underset{\sim}{\sigma}^I$), the average plastic strain tensor ($\underset{\sim}{\varepsilon}^p$) and the plastic strain tensor in the inclusion ($\underset{\sim}{\varepsilon}^{pI}$) [7]. The expression of equation 1 is valid for uniform elasticity:

$$\underset{\sim}{\sigma} = \underset{\sim}{\sigma}^I + \underset{\approx}{C} : \left(\underset{\sim}{\varepsilon}^p - \underset{\sim}{\varepsilon}^{pI}\right) \tag{1}$$

The fourth order tensor $\underset{\approx}{C}$ depends on the elastic properties and of the shape of the inclusions. As classically shown [8], the corresponding accommodation is elastic, so that the residual stresses (*id est* the difference between the average stress and the stress in the inclusion) are too large. The residual stress level is valid at the onset of plastic deformation in the inclusion, nevertheless, a more realistic evaluation for larger plastic strains must involve a plastic accommodation. This is the case in the self-consistent approach developed by Hill [9], and also in the "β–rule" proposed by Cailletaud and Pilvin [10, 11]. The interest of this last model is to preserve an explicit formulation. The idea is just to replace the plastic strain by an auxiliary variable, with a non linear evolution, so that the amount of residual stress is limited. The plastic strain in the inclusion is replaced by a variable $\underset{\sim}{\beta}^I$. The average of $\underset{\sim}{\beta}^I$ on the whole aggregate is $\underset{\sim}{\beta}$, and:

$$\dot{\underset{\sim}{\beta}}^I = \dot{\underset{\sim}{\varepsilon}}^{pI} - \underset{\approx}{D} : \left(\underset{\sim}{\beta}^I - \underset{\approx}{\delta} : \underset{\sim}{\varepsilon}^{pI}\right) ||\dot{\underset{\sim}{\varepsilon}}^{pI}|| \tag{2}$$

Unlike Kröner's or Hill's models, this approach has adjustable scale transition parameters. The shape of the tensors can be customized to take into account various types of materials (see for instance an application to directionnally solidified alloys in [12]). The purpose of the present paper is to investigate a possible extension of

the model to a finite body with a free surface. The plastic zone at the notch tip is nothing but a specific inclusion, and the zone surrounding this material element plays the role of the equivalent medium. The fourth order tensors $\underset{\approx}{C}$, $\underset{\approx}{D}$ and $\underset{\approx}{\delta}$ have to be determined from FEA. For a tension-torsion loading on the longitudinal axis 2 of a test specimen, the shape of these tensors is the following in Voigt notation: in our case $(1, 2, 3) \equiv (r, z, \theta)$. Only a few components of the stress and strain tensors are non zero. The tensor $\underset{\approx}{\delta}$ is just a diagonal:

$$\underset{\sim}{\sigma} \equiv \begin{pmatrix} 0 \\ \sigma_2 \\ \sigma_3 \\ 0 \\ \sigma_5 \\ 0 \end{pmatrix} \quad \underset{\sim}{\varepsilon} \equiv \begin{pmatrix} \varepsilon_1 \\ \varepsilon_2 \\ \varepsilon_3 \\ 0 \\ \varepsilon_5 \\ 0 \end{pmatrix} \quad \underset{\approx}{\delta} \equiv \begin{pmatrix} \delta_1 & 0 & 0 & 0 & 0 & 0 \\ 0 & \delta_1 & 0 & 0 & 0 & 0 \\ 0 & 0 & \delta_1 & 0 & 0 & 0 \\ 0 & 0 & 0 & \delta_2 & 0 & 0 \\ 0 & 0 & 0 & 0 & \delta_2 & 0 \\ 0 & 0 & 0 & 0 & 0 & \delta_2 \end{pmatrix} \tag{3}$$

Three lines and three colums in $\underset{\approx}{C}$ and $\underset{\approx}{D}$ are full of zeros to ensure a zero stress vector at the free surface.

$$\underset{\approx}{C} \equiv \begin{pmatrix} 0 & 0 & 0 & 0 & 0 & 0 \\ 0 & C_{22} & C_{23} & 0 & C_{25} & 0 \\ 0 & C_{23} & C_{33} & 0 & C_{35} & 0 \\ 0 & 0 & 0 & 0 & 0 & 0 \\ 0 & C_{25} & C_{35} & 0 & C_{55} & 0 \\ 0 & 0 & 0 & 0 & 0 & 0 \end{pmatrix} \quad \underset{\approx}{D} \equiv \begin{pmatrix} 0 & 0 & 0 & 0 & 0 & 0 \\ 0 & D_{22} & D_{23} & 0 & D_{25} & 0 \\ 0 & D_{23} & D_{33} & 0 & D_{35} & 0 \\ 0 & 0 & 0 & 0 & 0 & 0 \\ 0 & D_{25} & D_{35} & 0 & D_{55} & 0 \\ 0 & 0 & 0 & 0 & 0 & 0 \end{pmatrix} \tag{4}$$

These tensors are introduced in eq. 1, where the macroscopic plastic strain tensor has been set to zero, and the local plastic strain is replaced by $\underset{\sim}{\beta}^I$:

$$\underset{\sim}{\sigma} = \underset{\sim}{\sigma}^I - \underset{\approx}{C} : \underset{\sim}{\beta}^I \tag{5}$$

We have to determine 14 scale transition parameters, namely six in $\underset{\approx}{C}$, six in $\underset{\approx}{D}$, and two in $\underset{\approx}{\delta}$. This is made by means of:

- an elastic computation of the structure to evaluate the elastic stress state at the notch root for a prescribed load;
- an elastic-plastic computation providing the two or three first branches of the history of the local stresses and strains for the same repeated loading.

The von Mises plasticity criterion and a plastic flow deduced from the normality rule are coupled with a non-linear kinematic behaviour, described by parameters C and D [13]:

$$f\left(\underset{\sim}{\sigma}\right) = J\left(\underset{\sim}{\sigma} - \underset{\sim}{\mathbf{X}}\right) - R_0 \tag{6}$$

$$J\left(\underset{\sim}{\sigma}\right) = \left(\left(\frac{3}{2}\right) s_{ij} s_{ij}\right)^{1/2} \tag{7}$$

$$\dot{\underset{\sim}{\mathbf{X}}} = \frac{2}{3} C \dot{\underset{\sim}{\varepsilon}}^p - D \underset{\sim}{\mathbf{X}} \dot{p} \tag{8}$$

$$\dot{\underset{\sim}{\varepsilon}}^p = \dot{p} \frac{\partial f}{\partial \underset{\sim}{\sigma}} \tag{9}$$

Figure 1 illustrates the two corresponding FE computations.

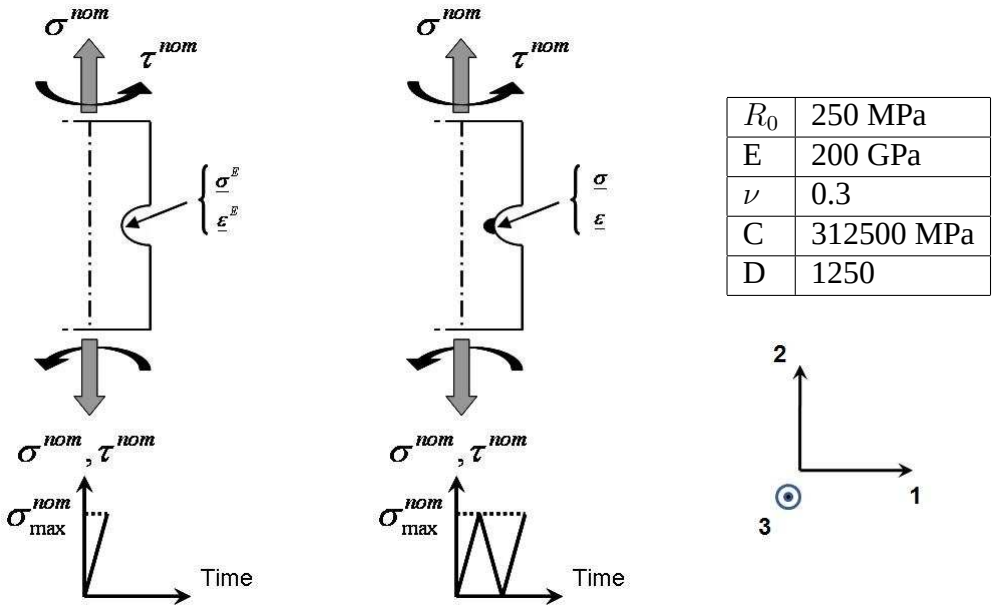

R_0	250 MPa
E	200 GPa
ν	0.3
C	312500 MPa
D	1250

a: Elastic regime b: Elastic-plastic regime

Figure 1: Description of the finite element analyses used to calibrate the model

3 Comparison between the model predictions and reference FEA

Finite Element analyses have been performed on an axisymmetric notched specimen with the code ZSeT/ZeBuLoN [14]. This geometry has been chosen since most of the simplified models do not predict a correct local response in this case. Neuber's method is really efficient only for uniaxial stress states, and even more recent methods [6] hardly predict the component σ_3 in this case, even if σ_2 is generally well captured. The core diameter is 9.2 mm; the diameter at the notch root is 7 mm. The radius of the notch is 0.4 mm. The stress concentration factor in tension (σ_2 at the notch root divided by σ_2 on the top of the specimen) is 5.28; the same

ratio computed for the case of a torsion loading (component σ_5) provides a value of 4.43. The results are used to make the identification of the scale transition parameters. The FE data base includes tension loadings, torsion loadings with several load ratios (R = 0, -0.3, -0.7) and finally combined proportional tension-torsion loading. The tension test is computed with an axisymmetric mesh. The elements are second order quadrilateral with reduced integration. One half of the 3D specimen is modeled by tetrahedral solid elements (10 nodes, 5 Gauss points) for the torsion case, meanwhile the full specimen is modeled for computing the combined loading. The three meshes are presented in figure 2. A convergence has been made to establish the relevant element size at the notch root. The value for the final mesh is 0.02 mm for the 2D mesh, and 0.14 mm for the 3D meshes. For each loading case, the FE results were read at the notch tip, on the x_1 axis. They are considered as a "numerical experiment", and the parameters of the simplified model are adjusted to reproduce the same curve. The capabilities of the optimizer embedded in ZSeT are used for that purpose.

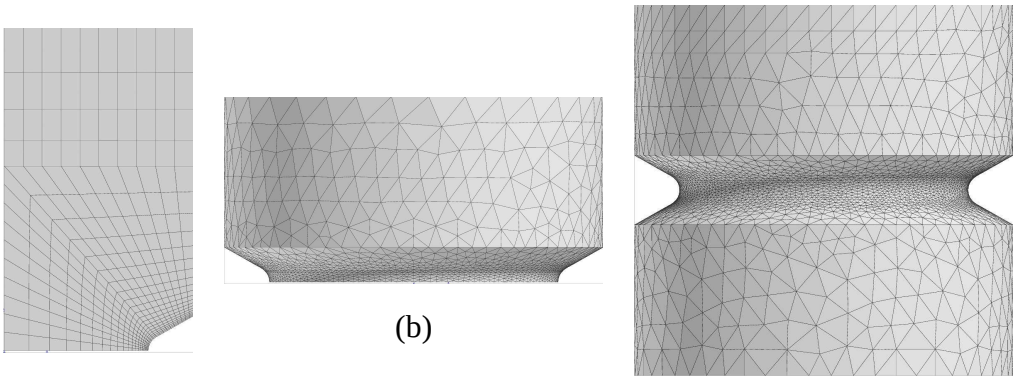

(a) (b) (c)

Figure 2: Meshes for the three loading cases: (a) Tension, 520 elements, 3330 dofs; (b) torsion, 20818 elements, 99966 dof; (c) Combined loading, 60905 elements, 267807 dof

3.1 Torsion loading

This kind of loading is quite simple since the only non-zero components in the stress and strain tensors are $\sigma_{23} = \sigma_5$ and $\varepsilon_{23} = \varepsilon_5$. A torque of 80 N.m is applied on the top of the mesh. In the FEA (mesh of Figure 2(b)), the geometric symmetry plane remains plane. It is then fixed in the three directions of the space. The model parameters have been optimized on the two first branches of a repeated torsion loading. The corresponding values are: $C_{55} = 101764.3$ MPa, $D_{55} = 1203.3$, $\delta_1 = 0.$, $\delta_2 = 0.425$.

Figure 3 (a) shows that the fit of the loop obtained by the model is rather good for the case used in the identification process. The parameters have then been used for the simulation of other loading cases, with R=-0.3 and R=-0.7. Figure 3 (b)

demonstrates that the model gives again a rather good approximation: even if the mean strain of the stabilized cycle is not the good one, Table 1 shows that the maximum stress of the steady state cycle is the good one, and the amplitudes of stress and strain are quite satisfactory. The critical variables used in the multiaxial fatigue prediction models are then well reproduced. The same result was confirmed with a loading at R=-0.7, that is not reproduced here for the sake of brevity.

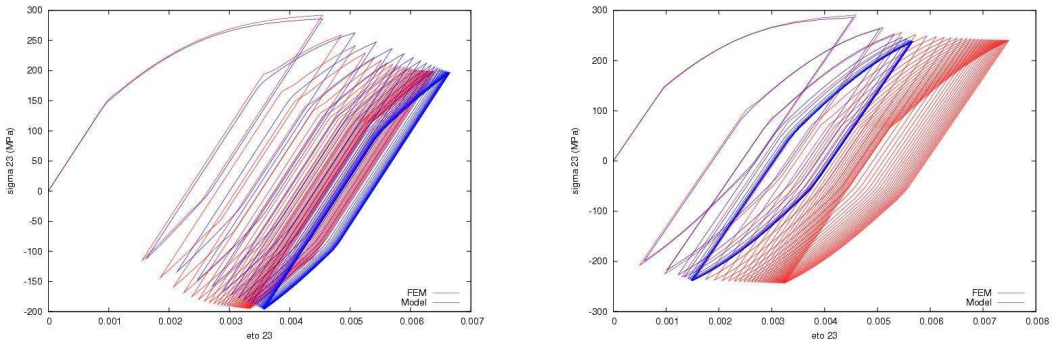

(a) (b)

Figure 3: Comparison of the local $\sigma_5 - \varepsilon_5$ histories obtained by FEA and the simplified model for a torsion loading: (a) R=0; (b) R=-0.3

	R = 0		R = -0.3		R = -0.7	
	FEM	Model	FEM	Model	FEM	Model
$\Delta\varepsilon_5$ (10^{-3})	3.34	3.06	4.26	4.17	6.27	6.21
$\overline{\varepsilon_5}$ (10^{-3})	4.87	5.12	5.36	3.58	4.21	1.54
$\Delta\sigma_5$ (MPa)	393.26	391.62	483.24	476.19	572.48	563.19
$\overline{\sigma_5}$ (MPa)	1.86	0.13	-1.4	0	-0.59	0

Table 1: Ranges and mean values of stresses and strains at the steady state obtained by FEA and the simplified model for a torsion loading

3.2 Tension loading

Here the symmetry plane is fixed in x_2 direction (mesh of Figure 2(a)), and a tensile force of 10.6 kN is applied on the top of the mesh. The equivalent stress state on the top surface is uniaxial, with a value of 160 MPa for σ_2. Unlike torsion case, there are now several non zero terms in the stress and strain tensors, namely $\sigma_2 = \sigma_{22}$ and $\sigma_3 = \sigma_{33}$, $\varepsilon_1 = \varepsilon_{11}$, $\varepsilon_2 = \varepsilon_{22}$ and $\varepsilon_3 = \varepsilon_{33}$. The model parameters have been identified on σ_2, σ_3, ε_2 and ε_3 of the three first branches of a repeated tension loading:

$C_{22} = 153136.9$ MPa	$C_{33} = 314938.6$ MPa	$C_{23} = 7076.9$ MPa
$D_{22} = 287.6$	$D_{33} = 8.7$	$D_{23} = 40.3$
$\delta_1 = 0.684$	$\delta_2 = 0.$	

The comparisons of the simplified method and of the FEA are given in Figures 4, 5 and Tables 2, 3 for the steady state cycle. The agreement is very good for the case that has been used for the identification (Fig. 4(a) and 5(a)). It is still quite satisfactory for the cases R=-0.3 and R=-0.7, which are pure predictions (Fig. 4(b) and 5(b)). Like for the previous case, there is only a slight difference on the mean strain, but all the other characteristics of the cycle are good.

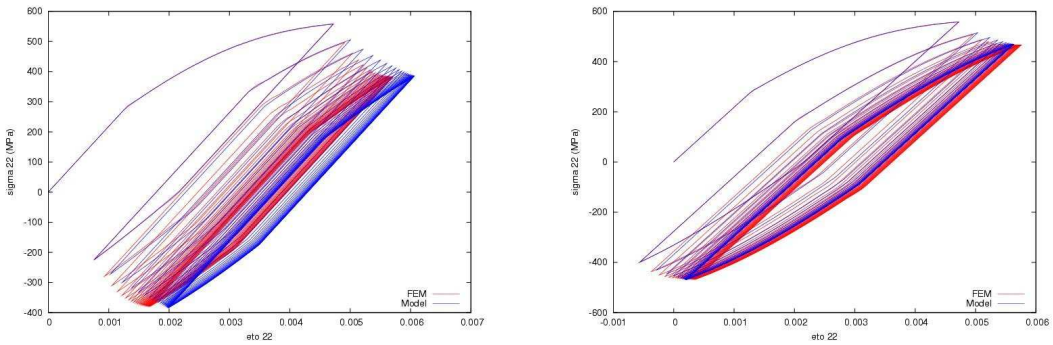

(a) (b)

Figure 4: Comparison of the local $\sigma_2 - \varepsilon_2$ histories obtained by FEA and the simplified model for a tension loading: (a) R=0; (b) R=-0.3

	R = 0		R = -0.3		R = -0.7	
	FEM	Model	FEM	Model	FEM	Model
$\Delta\varepsilon_2$ (10^{-3})	4.02	4.06	5.39	5.41	7.41	7.40
$\overline{\varepsilon_2}$ (10^{-3})	3.70	4.03	3.06	2.92	1.68	1.25
$\Delta\sigma_2$ (MPa)	760.22	766.34	932.35	936.04	1099.12	1098.76
$\overline{\sigma_2}$ (MPa)	1.52	0.31	-0.78	-0.06	-0.28	-0.02

Table 2: Ranges and mean values of stresses and strains at the steady state obtained by FEA and the simplified model for a tension loading on axis 2

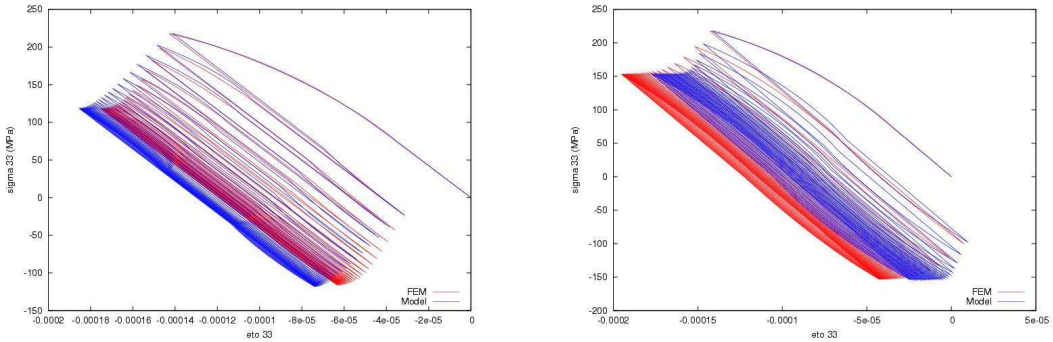

(a) (b)

Figure 5: Comparison of the local $\sigma_3 - \varepsilon_3$ histories obtained by FEA and the simplified model for a tension loading: (a) R=0; (b) R=-0.3

	R = 0		R = -0.3		R = -0.7	
	FEM	Model	FEM	Model	FEM	Model
$\Delta\varepsilon_3$ (10^{-4})	-1.12	-1.12	-1.53	-1.54	-2.16	-2.20
$\overline{\varepsilon_3}$ (10^{-4})	-1.19	-1.30	-1.19	-1.00	-0.758	-0.551
$\Delta\sigma_3$ (MPa)	234.6	236.84	306.9	307.79	399.56	398.11
$\overline{\sigma_3}$ (MPa)	1.08	0.2	-0.14	-0.22	-0.09	-0.08

Table 3: Ranges and mean values of stresses and strains at the steady state obtained by FEA and the simplified model for a tension loading on axis 2

3.3 Combined tension-torsion loading

The model parameters have been identified on the three first branches of a repeated tension-torsion proportional loading:

$C_{22} = 133478.7$ MPa	$C_{33} = 544048.1$ MPa	$C_{23} = 98024.0$ MPa
$C_{55} = 98718.0$ MPa	$C_{25} = 9079.3$ MPa	$C_{35} = 29144.9$ MPa
$D_{22} = 212.1$	$D_{33} = 3.3$	$D_{23} = 92.0$
$D_{55} = 3744.4$	$D_{25} = 10.4$	$D_{35} = 9.4$
$\delta_1 = 0.75$	$\delta_2 = 0.375$	

Here the test specimen is subjected to a tensile force of 7.0 kN and a torque of 56 N.m. Figure 6 and Table 4 show the comparison between the FEA and the simplified method, for the $\sigma_2 - \varepsilon_2$ loop (Fig. 6(a)) and for $\sigma_5 - \varepsilon_5$ (Fig. 6(b)). The agreement is rather good.

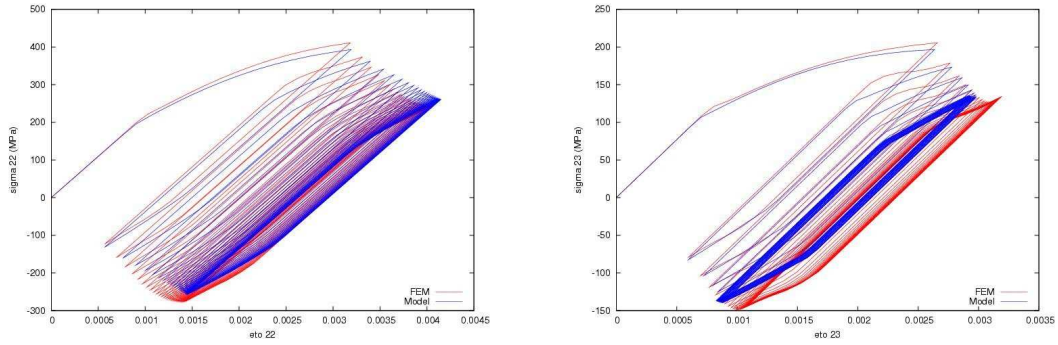

(a) (b)

Figure 6: Comparison of the hysteresis loops obtained by FEA and the simplified model for a tension–torsion loading at R=0: (a) $\sigma_2 - \varepsilon_2$; (b) $\sigma_5 - \varepsilon_5$

	FEM	Model
$\Delta\varepsilon_2$ (10^{-3})	2.65	2.69
$\overline{\varepsilon_2}$ (10^{-3})	2.75	2.80
$\Delta\sigma_2$ (MPa)	522.75	515.14
$\overline{\sigma_2}$ (MPa)	-14.62	1.47

(a)

	FEM	Model
$\Delta\varepsilon_5$ (10^{-3})	2.09	2.09
$\overline{\varepsilon_5}$ (10^{-3})	2.15	1.87
$\Delta\sigma_5$ (MPa)	275.26	271.59
$\overline{\sigma_5}$ (MPa)	-3.64	-0.55

(b)

Table 4: Comparison of ranges and mean values of stresses and strains obtained by FEA and the simplified model for a tension–torsion loading at R=0

4 Concluding remarks

In this paper, we developed a new method based on an adjustable scale transition rule to evaluate the local stress and strain states at a notch root. The method was tested under tension, torsion and combined proportional tension-torsion loadings, with different stress ratios. The model predictions are in good agreement with FEA results, even for the orthoradial stress–strain loops. For all the cases, the stress redistribution, the related local ratchetting and the final mechanical steady state are well described. These results are quite encouraging, and show that the output of the simplified model can then be taken as the input of a multiaxial fatigue analysis.

Further developments will include a more detailed study of the $\underset{\approx}{\delta}$ tensor, suppression of non significant parameters of $\underset{\approx}{C}$ and $\underset{\approx}{D}$, and the identification of the model on a larger data base, including several load amplitudes and non proportional loading paths. The physical meaning of the parameters of the transition rule will be also considered.

References

[1] P. Lesne, S. Savalle, 2nd Int. Conf. on Computational Plasticity (Sept. 18-22, 1989) 591–602.

[2] H. M. Maitournam, B. Pommier, J. J. Thomas, C.R. Mécanique 330 (2002) 703–708.

[3] H. Neuber, Theory of stress concentration for shear-strained prismatical bodies with arbitrary nonlinear stress-strain law, J. of Applied Mechanics (1961) 544–550.

[4] K. Molski, G. Glinka, A method of elastic-plastic stress and strain calculation at a notch root, Material Science and Engineering 50 (1981) 93–100.

[5] A. Moftakhar, A. Buczynski, G. Glinka, Calculation of elasto-plastic strains and stresses in notches under multiaxial loading, Int. J. Frac 70 (1995) 357–373.

[6] A. Buczynski, G. Glinka, An analysis of elasto-plastic strains and stresses in notched bodies subjected to cyclic non-proportional loading paths, Biaxial/Multiaxial Fatigue and Fracture (2003) 265–283.

[7] E. Kröner, Zur plastischen verformung des vielkristalls, Acta Metall. 9 (1961) 155–161.

[8] M. Berveiller, A. Zaoui, An extension of the self–consistent scheme to plastically flowing polycrystal, J. Mech. Phys. Sol. 26 (1979) 325–344.

[9] R. Hill, A self–consistent mechanics of composite materials, J. Mech. Phys. Sol. 13 (1965) 213–222.

[10] G. Cailletaud, Une approche micromécanique phénoménologique du comportement inélastique des métaux, Ph.D. thesis, Université Pierre et Marie Curie, Paris 6 (1987).

[11] G. Cailletaud, P. Pilvin, Utilisation de modèles polycristallins pour le calcul par éléments finis, Revue Européenne des Éléments Finis 3 (4) (1994) 515–541.

[12] K. Sai, G. Cailletaud, S. Forest, Micro-mechanical modeling of the inelastic behavior of directionally solidified materials, Mech. of Materials 38 (2006) 203–217.

[13] J. Lemaitre, J. L. Chaboche, Mécanique des Matériaux Solides, Dunod, 1985.

[14] J. Besson, R. Le Riche, R. Foerch, G. Cailletaud, Object–oriented programming applied to the finite element method. Part II: Application to material behaviors, Revue Européenne des Éléments Finis 7 (5) (1998) 567–588.